Geophysical and Astrophysical Fluid Dynamics
Vol. 00, No. 00, 00 Month 2012, 1–16

Balanced Convective Circulations in a Stratified Atmosphere. Part II: Circulations in the Presence of Radiation and the Non-Traditional Coriolis Terms

David H. Marsico†*, Joseph A. Biello †, and Matthew R. Igel ‡

† Department of Mathematics, University of California Davis, Davis, California
‡Department of Land, Air, and Water Resources, University of California Davis, Davis, California

(*v4.4 released October 2012*)

The full Coriolis force consists of terms proportional to the sine and cosine of latitude. The latter, referred to as the non-traditional Coriolis terms, couple the zonal and vertical momentum equations, and are often neglected. When considering the incompressible Euler equations at the equator in the presence of the full Coriolis force, it can be shown that all dynamical fields can be diagnosed from the velocity potential, which itself is the solution to an elliptic equation that depends on latitude, momentum drag, and radiative damping. In this work, we present solutions to these equations for several different types of momentum drag and radiative damping. An important insight of our work is the combined effect that both rotation and radiation have on providing a mechanism for ascent and descent of air away from a localized source of heating.

Keywords: Coriolis Force; Radiation; Convection; Weak Temperature Gradient; Rotation

1. Introduction

In a companion paper (Marsico *et al.* 2023), we developed an approximation to the primitive equations in order to derive a convective parameterization framework that we called the Convective Weak Temperature Gradient equations (C-WTG). To do so, we examined the incompressible Euler equations on convective length scales and sub-diurnal time scales. Considering low Rossby number flows, we suggested a simple drag parameterization for the turbulent damping associated with advective nonlinearity (Romps and Charn 2015, Jeevanjee and Romps 2016). Since hydrostatic balance is not appropriate on horizontal length scales associated with convection, we showed how both traditional and non-traditional terms in the Coriolis force can have an effect on steady circulations. The C-WTG equations we derived depend on latitude, θ, and take the form

*Corresponding author. Email: david.marsico@noaa.gov

$$-2\Omega\sin(\theta)v + 2\Omega\cos(\theta)w = -\frac{\partial\phi}{\partial x} - d_1 u \tag{1a}$$

$$2\Omega\sin(\theta)u = -\frac{\partial\phi}{\partial y} - d_1 v \tag{1b}$$

$$-2\Omega\cos(\theta)u = -\frac{\partial\phi}{\partial z} + b - d_1 w \tag{1c}$$

$$N^2 w = S - d_2 b, \tag{1d}$$

$$\nabla\cdot\boldsymbol{u} = 0, \tag{1e}$$

These equations constitute a steady, linear f-plane approximation of the stratified Euler equations. The zonal, meridional, and vertical components of the velocity are (u, v, w), the buoyancy, b, and the pressure in the Boussinesq approximation is $\phi = p/\rho_0$, where ρ_0 is a reference density. The latitude of the f-plane is θ, the rotation rate of the Earth, Ω, the buoyancy frequency is $N \approx 2\times10^{-2}$ s^{-1}, and the rate of input of buoyancy from latent heating is S. In this approximation (and in the actual atmosphere), non-linear turbulent dissipation far exceeds molecular dissipation, and for convection, occurs below the scales considered by this framework. Dissipative effects are approximated with Newtonian drag (with rate d_1), and cooling (rate d_2).

Marsico *et al.* (2023) develop this approximation by considering a scale analysis and dominant balance of the stratified, incompressible Navier-Stokes equations. Earth's rotation rate sets a time scale $(2\Omega)^{-1}$ of approximately 2 hours, the depth of the troposphere sets a length scale on the order 7 km, and together these yield a velocity of 1 m s^{-1}. Momentum and radiative damping time scales which are on the order of 2 hours are consistent with this approximation, and are on the order of a convective turnover time for the troposphere. Marsico *et al.* (2023) discuss how the drag damping can be straightforwardly generalized to turbulent dissipation and how this linear framework can be extended to a non-linear, steady framework.

A case of particular interest occurs at the equator where only the non-traditional Coriolis Terms (NCTs) are the only Coriolis terms present. Setting $\theta = 0$ in equations (1a)-(1e), we obtain

$$2\Omega w = -\frac{\partial\phi}{\partial x} - d_1 u \tag{2a}$$

$$0 = -\frac{\partial\phi}{\partial y} - d_1 v \tag{2b}$$

$$-2\Omega u = -\frac{\partial\phi}{\partial z} + b - d_1 w \tag{2c}$$

$$N^2 w = S - d_2 b \tag{2d}$$

$$\nabla\cdot\boldsymbol{u} = 0, \tag{2e}$$

where d_1 and d_2 are the momentum and thermal damping terms. This set of equations forms the basis for our current work, which is divided into three parts. First, we consider equations (2a)-(2e) in the case when $d_1 \neq 0$ and $d_2 = 0$. Second, we consider the case when both $d_1 \neq 0$ and $d_2 \neq 0$, and third, we extend the analysis to a case with linear thermal damping and diffusive momentum damping. We provide this progression for two reasons. The first is that it is not strictly obvious which case is the most relevant to atmospheric convective circulations. The second is that by providing progressively more complicated solutions we develop a more systematic understanding of the effect of each of the underlying physical processes.

We focus specifically on the linearized primitive equations with all Coriolis force terms because we believe the NCTs have not been analyzed as well as is warranted. We begin

by examining the solution in the case of a circular equatorial heating which is intended to represent equatorial convective heating, either from a single deep convective cloud or an organized convective system. We choose to present and contrast three different cases (as noted above) since it is not obvious which description of damping and radiation is most relevant on convective or mesoscales.

One of the main insights of our work is the importance of coupling between radiation and rotation, and how they relate to the response to a localized heating. In the absence of radiation, the equation for the vertical velocity simplifies to the fundamental equation of the weak temperature gradient (WTG) approximation; the direct diagnosis of vertical velocity from heating. In particular, a localized heating source results in a purely local response in the vertical velocity. However, when radiation is present, it couples rotation to the circulation in a way that induces a non-local response, and allows the flow to ascend and descend away from the source of the heating.

Our paper is organized as follows. In each section, we attempt to illustrate the most critical ways in which the energetics and flow responds to the relevant physics. We always show the response of the vertical velocity to an imposed heating. In cases where it is relevant, the horizontal flow will be discussed. In some cases, energetics will be mentioned. So, while different aspects of the response will be discussed in different sections, these differences are curated and intentional.

2. Linear Momentum Damping

As a first application, we consider equations (2a)-(2e) in the case that $d_2 = 0$, which is a common assumption. The inclusion of a linear momentum damping will allow steady circulations to be achieved as imposed heating is fully dissipated through friction. The shape of the heating and the magnitude of the damping will fully determine the resulting balanced flow. To solve the appropriate equations, we introduce the stream function, ψ, and velocity potential, Φ, and decompose the velocity field as (Helmholtz 1867, Lebovitz 1989)

$$\boldsymbol{u} = (-\Phi_x - \psi_y)\boldsymbol{i} + (-\Phi_y + \psi_x)\boldsymbol{j} + w\boldsymbol{k}, \tag{3}$$

where the subscripts x and y denote partial derivatives with respect to these variables. It is then straightforward to show that

$$\nabla_h^2 \Phi = w_z, \tag{4}$$

or equivalently

$$\nabla_h^2 \Phi = \frac{S_z}{N^2}, \tag{5}$$

and

$$\nabla_h^2 \psi = \frac{2\Omega w_y}{d_1}. \tag{6}$$

Here, $\nabla_h^2 = \partial_x^2 + \partial_y^2$ denotes the horizontal Laplacian. We use a simple choice of heating, S, that is localized about the origin and that vanishes at the bottom and top of the troposphere. In particular, we let

$$S = \begin{cases} f(z) & \text{if } r \leq L \\ 0 & \text{else,} \end{cases} \tag{7}$$

where $r = \sqrt{x^2 + y^2}$ is the horizontal radial coordinate and L is the radius of the region where the heating is applied. This form of the heating will allow us to write down exact solutions to

equations (2a)-(2e). Equations (4) and (6) can be solved to yield

$$\Phi = \begin{cases} \dfrac{1}{4N^2}(r^2 - L^2)f'(z) & \text{if } r \le L \\ \dfrac{L^2}{2N^2}f'(z)\ln(r/L) & \text{else} \end{cases} \tag{8}$$

and

$$\psi = \begin{cases} \dfrac{\Omega y}{d_1 N^2}f(z) & \text{if } r \le L \\ \dfrac{\Omega y L^2}{d_1 N^2 r^2}f(z) & \text{else.} \end{cases} \tag{9}$$

Here, $f'(z)$ denotes the derivative of f with respect to z. Therefore, the velocities are

$$u = \begin{cases} -\dfrac{x}{2N^2}f'(z) - \dfrac{\Omega}{d_1 N^2}f(z) & \text{if } r \le L \\ -\dfrac{L^2 x}{2N^2 r^2}f'(z) - \dfrac{2\Omega}{N^2}\left(\dfrac{L^2}{2d_1 r^2} - \dfrac{y^2 L^2}{d_1 r^4}\right)f(z) & \text{else} \end{cases} \tag{10}$$

$$v = \begin{cases} -\dfrac{y}{2N^2}f'(z) & \text{if } r \le L \\ -\dfrac{yL^2}{2N^2 r^2}f'(z) - \dfrac{2\Omega x y L^2}{d_1 N^2 r^4}f(z) & \text{else} \end{cases} \tag{11}$$

To compute ϕ, we integrate the meridional momentum equation. For $r > L$, we have

$$\begin{aligned} \phi &= \int_0^y \left[\frac{y' d_1 L^2}{2N^2 r^2}f'(z) + \frac{2\Omega x y' L^2}{N^2 r^4}f(z)\right] dy' \\ &= \frac{d_1 L^2}{4N^2}f'(z)\ln(r^2/x^2) + \frac{2\Omega L^2}{N^2}f(z)\left[-\frac{x}{2r^2} + \frac{1}{2x}\right] + g_1(x,z). \end{aligned} \tag{12}$$

When $r \le L$, we have

$$\begin{aligned} \phi &= \int_0^y \frac{d_1 y'}{2N^2}f'(z)\,dy' \\ &= \frac{d_1 y^2}{4N^2}f'(z) + g_2(x,z). \end{aligned} \tag{13}$$

To determine g_1 and g_2, we substitute the zonal velocity, the vertical velocity, and ϕ into the zonal momentum equation, (2a). For $r > L$, after some algebra and one integration we find

$$g_1 = \frac{d_1 L^2}{4N^2}f'(z)\ln(x^2/L^2) - \frac{\Omega L^2}{N^2 x}f(z) + f_1(z), \tag{14}$$

Similarly, for $r \le L$,

$$g_2 = -\frac{\Omega x}{N^2}f(z) + \frac{d_1 x^2}{4N^2}f'(z) + f_2(z). \tag{15}$$

For ϕ to be continuous across the heating discontinuity at $r = L$, we must have

$$f_1(z) = \frac{d_1 L^2}{4N^2}f'(z) + f_2(z). \tag{16}$$

Choosing $f_1(z)$ equal to zero amounts to removing the geopotential term independent of z in the far field, thus yielding a negative geopotential at the origin

$$\phi = \begin{cases} \dfrac{d_1\left(r^2 - L^2\right)}{4N^2} f'(z) - \dfrac{\Omega x}{N^2} f(z) & \text{if } r \leq L \\ \\ \dfrac{d_1 L^2}{4N^2} f'(z) \ln(r^2/L^2) - \dfrac{\Omega L^2 x}{N^2 r^2} f(z) & \text{else.} \end{cases} \tag{17}$$

The buoyancy is readily computed from the vertical momentum equation (2c)

$$b = \begin{cases} f(z)\left(\dfrac{2\Omega^2}{d_1 N^2} + \dfrac{d_1}{N^2}\right) + \dfrac{d_1\left(r^2 - L^2\right)}{4N^2} f''(z) & \text{if } r \leq L \\ \\ \dfrac{4\Omega^2}{N^2}\left(\dfrac{L^2}{2d_1 r^2} - \dfrac{y^2 L^2}{d_1 r^4}\right) f(z) + \dfrac{d_1 L^2}{4N^2} \ln(r^2/L^2) f''(z) & \text{else.} \end{cases} \tag{18}$$

2.1. *Discussion*

Considering flows in the absence of radiative damping means that equation (2d) amounts to the weak temperature gradient approximation (WTG) on convective scales (Hittmeir and Klein 2018). We choose a vertical heating profile, $f(z)$, to be consistent with a mid tropospheric extremum, and vanishing heating in the lower and upper troposphere, $f(z) = S_0 \sin(\pi z/H)$, where $S_0 = 10^{-4}\,\mathrm{m\,s^{-3}} = 0.36\,\mathrm{m\,s^{-2}\,hr^{-1}}$, $z \in (0, H)$, and $H = 15$ km is the height of the troposphere. We also set $L = H$ in equation (7), so that the radius of the region of non-zero heating is equal to the height of the troposphere. We use damping coefficients of $d_1 = 0.1\,\mathrm{s^{-1}}$, and $d_1 = 10^{-5}\,\mathrm{s^{-1}}$, which correspond to the strong and weak damping limits. Plots are shown at heights of $z = 0, H/2, H$. From figure 1, which corresponds to $d_1 = 0.1\,\mathrm{s^{-1}}$, we see that the buoyancy, b, is zero at $z = 0$ and $z = H$, which correspond to the bottom and top of the troposphere. From equation (18), we see that in the mid-troposphere, the buoyancy is radially symmetric within the heating region, but non-symmetric outside of it. However, for the relatively strong damping coefficient of $d_1 = 0.1\,\mathrm{s^{-1}}$ we are considering, this asymmetry, induced by the non-traditional Coriolis terms, is damped out, and the buoyancy is essentially as symmetric in figure 1.

Again from figure 1, we see that at the bottom (top) of the troposphere, the horizontal velocity converges toward (diverges away from) the heating region. The meridional winds are confluent to the east of the heating and difluent to the west. This pattern closely resembles that discussed as arising around a convective cloud under the influence of the NCT (Igel and Biello 2020) or as a result of synoptic-scale equatorial heating (Hayashi and Itoh 2012). In the mid-troposphere, the velocity is relatively weak, owing again to a strong damping coefficient (equation 6).

Figure 2 more clearly illustrates the nature of the horizontal flow. At $z = 0$ and $z = H$, the flow is entirely described by the potential. This implies that the flow is purely confluent and difluent. In the mid-troposphere, the potential is everywhere zero but the stream function is not. This implies that the horizontal flow is entirely vortical at mid-levels as meridional planetary vorticity has been tilted into the vertical direction by the buoyancy-driven convection.

Figure 3 mimics 1 but for $d_1 = 10^{-5}\,\mathrm{s^{-1}}$, corresponding to a damping timescale of approximately one day. At the bottom and top of the troposphere, the zonal and meridional velocities are identical to what they are for $d_1 = 0.1\,\mathrm{s^{-1}}$, owing to the fact that here, they depend only on the velocity potential, which is independent of momentum damping. In the mid-troposphere,

they are qualitatively similar to what they are in figure 1, but differ in magnitude, which is due to the inverse dependence of the stream function on d_1. The buoyancy at the bottom and top of the troposphere are zero, but in the mid-troposphere it is now manifestly asymmetric, and zonal winds are westward everywhere there is positive buoyancy and negative everywhere there is negative buoyancy.

We can again understand the behavior of the horizontal velocities by looking at the stream function and velocity potential in figure 4. The velocity potential is independent of d_1, but the stream function is proportional $1/d_1$. So for weak momentum damping, the stream function will produce the relatively strong horizontal velocities seen in the mid-troposphere in figure 3.

3. Linear Momentum Damping and Newtonian Cooling

We now incorporate a Newtonian cooling term in the form of a constant, non-zero d_2. As was shown in Part I (Marsico *et al.* 2023), when $d_1 d_2 \ll N^2$, the equation for the velocity potential is

$$\nabla_h^2 \Phi + \frac{4\Omega^2}{N^2}\frac{d_2}{d_1}\Phi_{yy} = \frac{S_z}{N^2}. \tag{19}$$

3.1. *Redevelopment*

We now describe briefly how (19) was derived in (Marsico *et al.* 2023). First, we note that the vertical component of the curl of equation (3) results in the equation

$$\nabla_h^2 \psi = v_x - u_y. \tag{20}$$

Next, we eliminate the horizontal pressure gradient from equations (1a) and (1b) and use equations (1e), and (4) to obtain the extremely simple relationship between the velocity potential and stream function

$$d_1 \frac{\partial \psi}{\partial z} = 2\Omega \frac{\partial \Phi}{\partial n}, \tag{21}$$

where

$$\frac{\partial}{\partial n} = \cos(\theta)\frac{\partial}{\partial y} + \sin(\theta)\frac{\partial}{\partial z}. \tag{22}$$

At the equator, where $\theta = 0$, we have $\Phi_n = \Phi_y$. Equation (21) then simplifies to

$$d_1 \frac{\partial \psi}{\partial z} = 2\Omega \frac{\partial \Phi}{\partial y}. \tag{23}$$

We can use equations (20) and (21) as follows. Using equations (1a)-(1c), as well as the incompressibility equation (1e), we eliminate the pressure gradient and buoyancy to derive an equation for vertical velocity, w, in terms of the vertical component of vorticity, $v_x - u_y$, and the heating S. We then use equations (4), (20), and (21) to eliminate the vertical velocity and vorticity component in favor of the velocity potential, Φ. This results in the single equation for Φ at an arbitrary latitude θ:

$$\nabla_h^2 \Phi + \frac{d_1 d_2}{N^2 + d_1 d_2}\left[\Phi_{zz} + \left(\frac{2\Omega}{d_1}\right)^2 \Phi_{nn}\right] = \frac{S_z}{(N^2 + d_1 d_2)}. \tag{24}$$

At the equator, where $\theta = 0$, $\Phi_{nn} = \Phi_{yy}$. When $d_1 d_2 \ll N^2$, we can neglect the z-derivative term Φ_{zz} in the previous equation, and equation (19) follows.

3.2. *Solution*

To solve equation (19), we begin by defining

$$\alpha^2 = \frac{4\Omega^2}{N^2}\frac{d_2}{d_1}, \tag{25}$$

equation (19) becomes

$$\Phi_{xx} + (1+\alpha^2)\,\Phi_{yy} = \frac{S_z}{N^2} \tag{26}$$

We rescale the y variable as

$$Y = \frac{y}{\sqrt{1+\alpha^2}} \tag{27}$$

to yield the Poisson equation

$$\Phi_{xx} + \Phi_{YY} = \frac{S_z}{N^2}. \tag{28}$$

Now we need to specify the heating function. Let's choose

$$S(x,y,z) = S_0\ \sin(\pi z/H)\ \Theta(L - \sqrt{x^2+y^2}) \tag{29}$$

where Θ is the function defined by

$$\Theta(s) = \begin{cases} 1 & \text{if } s > 0 \\ 0 & \text{else.} \end{cases} \tag{30}$$

Therefore the heating is non-zero in a disk of radius L and zero elsewhere. In the new coordinates, the heating is nonzero when

$$\frac{x^2}{L^2} + \frac{Y^2}{\frac{L^2}{(1+\alpha^2)}} = 1 \tag{31}$$

which is an ellipse of semi-major axis L and semi-minor axis $L/(\sqrt{1+\alpha^2})$. Notice that the focus of the ellipse is located at $\alpha L/(\sqrt{1+\alpha^2})$. So while our rescaling of the variables has simplified the operator, we are left with an elliptical heating region instead of a circular one. If we define Φ such that

$$\Phi = \frac{\pi S_0}{HN^2}\ \cos(\pi z/H)\ F(x,y), \tag{32}$$

then the horizontal dependence of Φ, $F(x,y)$, solves the equation

$$F_{xx} + F_{YY} = \Theta(L - \sqrt{x^2 + (1+\alpha^2)\,Y^2}). \tag{33}$$

In order to solve equation (33), we introduce confocal elliptic coordinates:

$$x = \frac{\alpha L}{\sqrt{1+\alpha^2}}\cosh(\mu)\cos(\nu) \tag{34}$$

$$Y = \frac{\alpha L}{\sqrt{1+\alpha^2}}\sinh(\mu)\sin(\nu) \tag{35}$$

where

$$\left(\frac{x}{\frac{\alpha L\cosh(\mu)}{\sqrt{1+\alpha^2}}}\right)^2 + \left(\frac{Y}{\frac{\alpha L\sinh(\mu)}{\sqrt{1+\alpha^2}}}\right)^2 = 1, \tag{36}$$

and $0 \leq \nu < 2\pi$ and $\mu > 0$. Combining equations (34), (35), and (36) shows that the boundary is given by the equation

$$\sinh(\mu) = \alpha^{-1}. \tag{37}$$

We use μ_0 to denote the solution to the previous equation. A particular solution to equation (33) on the interior, that is, where $x^2 + (1+\alpha^2)Y^2 < L^2$, is given by F_p, where

$$F_p = \frac{1}{2\left(2+\alpha^2\right)}\left[x^2 + \left(1+\alpha^2\right)Y^2\right]. \tag{38}$$

We will add another harmonic function to this particular solution later. Note that the value of the particular solution on the boundary, F_0, is

$$F_0 = \frac{L^2}{2\left(2+\alpha^2\right)} \tag{39}$$

which is constant.

In confocal coordinates, the value of F_p in the interior is

$$F_p = \frac{\alpha^2 L^2}{2\left(2+\alpha^2\right)}\left[\frac{\cosh^2(\mu)\cos^2(\nu)}{1+\alpha^2} + \sinh^2(\mu)\sin^2(\nu)\right], \tag{40}$$

which, after some manipulation simplifies to

$$F_p = \frac{\alpha^2 L^2}{4\left(1+\alpha^2\right)\left(2+\alpha^2\right)}\left[\cosh^2(\mu) + \left(1+\alpha^2\right)\sinh^2(\mu) + \cos(2\nu)\left(1-\alpha^2\sinh^2(\mu)\right)\right]. \tag{41}$$

The normal derivative at the boundary is

$$\frac{\partial F_p}{\partial \mu} = \cosh(\mu)\sinh(\mu)\frac{\alpha^2 L^2}{\left(2+\alpha^2\right)}\left[\frac{\cos^2(\nu)}{1+\alpha^2} + \sin^2(\nu)\right], \tag{42}$$

which, evaluated at the boundary, becomes

$$\left.\frac{\partial F_p}{\partial \mu}\right|_{\mu_0} = \frac{L^2\left[2+\alpha^2-\alpha^2\cos(2\nu)\right]}{2\left(2+\alpha^2\right)\sqrt{1+\alpha^2}}. \tag{43}$$

Notice that the boundary value of the particular solution of the interior is independent of ν, but the derivative depends on $\cos(2\nu)$. In the exterior, where $x^2 + (1+\alpha^2)Y^2 > L^2$, equation (33) is simply Laplace's equation in confocal elliptical coordinates,

$$F_{\mu\mu} + F_{\nu\nu} = 0. \tag{44}$$

Thus, the solution in the exterior, denoted by F_{exterior}, is a linear combination of harmonic functions, and the interior and exterior solutions take the form

$$\begin{aligned} F_{\text{exterior}} &= c_0 + c_1\left(\mu - \mu_0\right) + c_2 e^{-2\mu}\cos(2\nu) \\ F_{\text{interior}} &= F_p + c_3\cosh(2\mu)\cos(2\nu) \end{aligned} \tag{45}$$

Matching the exterior solution to the interior solution yields

$$F_0 = c_0, \qquad c_3\cosh(2\mu_0) = c_2 e^{-2\mu_0}. \tag{46}$$

Matching the derivative yields

$$c_1 = \frac{\left(2+\alpha^2\right)L^2}{2\left(2+\alpha^2\right)\sqrt{1+\alpha^2}} \tag{47}$$

and

$$2c_3\sinh(2\mu_0) - \frac{\alpha^2 L^2}{2\left(2+\alpha^2\right)\sqrt{1+\alpha^2}} = -2c_2 e^{-2\mu_0}. \tag{48}$$

Solving for c_2, c_3 we find

$$c_2 = \frac{\alpha^2 L^2 \cosh(2\mu_0)}{4\,(2+\alpha^2)\,\sqrt{1+\alpha^2}} \tag{49}$$

$$c_3 = \frac{\alpha^2 L^2 e^{-2\mu_0}}{4\,(2+\alpha^2)\,\sqrt{1+\alpha^2}}. \tag{50}$$

Therefore, the exterior solution is

$$F_{\text{exterior}} = \frac{L^2}{2\,(2+\alpha^2)}\left[1 + \frac{(2+\alpha^2)}{\sqrt{1+\alpha^2}}\,(\mu-\mu_0) + \frac{\alpha^2}{2\sqrt{1+\alpha^2}}\cosh(2\mu_0)e^{-2\mu}\cos(2\nu)\right], \tag{51}$$

and the interior solution is

$$\begin{aligned} F_{\text{interior}} = \frac{\alpha^2 L^2}{4\,(1+\alpha^2)\,(2+\alpha^2)}\,&\left[\cosh^2(\mu) + \left(1+\alpha^2\right)\sinh^2(\mu)\right. \\ &\left. + \cos(2\nu)\left(1 + \sqrt{1+\alpha^2}e^{-2\mu_0}\cosh(2\mu) - \alpha^2\sinh^2(\mu)\right)\right], \end{aligned} \tag{52}$$

which in terms of x and Y is

$$F_{\text{interior}} = \frac{x^2 + \left(1+\alpha^2\right)Y^2}{2\,(2+\alpha^2)} + \frac{\sqrt{1+\alpha^2}e^{-2\mu_0}}{2\,(2+\alpha^2)}\left[x^2 - Y^2\right] - \frac{\alpha^2 L^2\sqrt{1+\alpha^2}e^{-2\mu_0}}{4\,(1+\alpha^2)\,(2+\alpha^2)}. \tag{53}$$

The velocity potential is thus given by the equation (32) where F is either the interior (equation 53) or exterior (equation 51) solution.

Given the velocity potential, we can easily solve for the vertical velocity, which is related to the velocity potential by the equation

$$w = \int_0^z \nabla_h^2\,\Phi(x,y,z')\,dz'. \tag{54}$$

From equation (19), we know that

$$\Phi_{xx} + \Phi_{yy} = \frac{S_z}{N^2} - \alpha^2\,\Phi_{yy}. \tag{55}$$

Integrating both sides of this identity with respect to z, and making use of equation (54), we obtain

$$\begin{aligned} w &= \int_0^z \left[\frac{S_z}{N^2} - \alpha^2\,\Phi_{yy}\right] dz' \\ &= \frac{S_0}{N^2}\sin(\pi z/H)(\Theta(L-\sqrt{x^2+y^2}) - \alpha^2 F_{yy}), \end{aligned} \tag{56}$$

where F is defined by equations (51) and (53). In terms of Y, w is expressed as

$$w = \frac{S_0}{N^2}\sin(\pi z/H)\left(\Theta(L-\sqrt{x^2+y^2}) - \frac{\alpha^2}{1+\alpha^2}F_{YY}\right). \tag{57}$$

Explicit expressions for the horizontal dependence of w given in confocal coordinates are provided in the appendix.

3.3. *Discussion*

Here we describe the qualitative features of the velocities, stream function, and velocity potential as functions of the parameter α^2 for a range of different values, as it is not necessarily clear which values of this parameter would be relevant in the real atmosphere. In figure 5, we plot the velocity potential at the bottom of the troposphere, $z = 0$, for increasing values of

α^2. Note that the velocity potential is anti-symmetric about the mid-troposphere, $z = H/2$, where it is everywhere zero. For small values of α^2, we see that the velocity potential is similar in structure to what it was in the absence of radiation. This is not unsurprising, as for fixed d_1, we can regard the regime $\alpha^2 \ll 1$ as corresponding to a weak radiation limit. However, as α^2 increases, that is to say, as the effects of radiation begin to be felt, the potential becomes more elliptic in shape with a semi-major axis in the meridional direction.

Figure 6 shows the vertical velocity as a function of α^2. On the interior, the velocity is constant and decreases in magnitude as α^2 increases. The vertical velocity outside of the heating region displays a pronounced sensitivity to α^2. In particular, for small values of α^2, the solution resembles that of the WTG approximation: a constant nonzero value on the interior and zero outside. However, as α^2 increases, noticeable regions of negative vertical velocity appear along the equator, and regions of positive vertical velocity appear poleward, with the amplitude in each of the regions increasing as α^2 increases. Furthermore, these exterior regions of non-zero vertical velocity become more elliptical in nature.

In figure 7, we plot the deviation of the vertical velocity from the weak temperature gradient solution, that is, the solution that is constant in the interior of the heating region and zero outside of it. This allows us to examine the effect that the non-traditional Coriolis terms have on the WTG solution. From figure 7, we see that the deviation is negative on the interior of the heating region, and thus serves to damp the WTG solution on the interior. On the exterior, we see the same regions of positive and negative vertical velocity that were observed in figure 6. Thus, it is the inclusion of the non-traditional Coriolis terms that provides a mechanism for ascent and descent away from a localized source of heating. It is also important to recognize the unique role that radiation plays in inducing this non-locality of the vertical velocity. Radiation is necessary for the non-traditional Coriolis terms to affect the vertical velocity, as when we set $d_2 = 0$ in equation (19), we recover the WTG solution for vertical velocity.

In figure 8, the interior velocity, a constant for any α^2, and the normalized domain integrated vertical velocity are plotted as a functions of α. The domain integrated vertical velocity is normalized by the area of the heating region so that it is equal to the interior vertical velocity for $\alpha^2 = 0$. Both the interior and domain integrated velocities monotonically decrease as a function of α^2 because the increase in thermal damping (at least relative to momentum damping) increasingly offsets the heating imposed in within $r = L$. As thermal damping becomes large relative to momentum damping, the area surrounding the heated region can cool and subside effectively without being influenced through momentum, as strongly as it is within the heating region.

In figure 9, we plot the stream function in the mid-troposphere for increasing values of α^2, for a fixed momentum damping coefficient of $d_1 = 10^{-5}\,\mathrm{s}^{-1}$. For small values of α^2, the stream function is similar to what it was in the absence of radiation, as can be seen by comparing it with the stream function in figure 4. The horizontal velocity can be understood by looking at figure 10, which shows both the stream function and corresponding vector field whose components are the zonal and meridional velocities. As was the case in the absence of radiation, the horizontal velocity in the mid-troposphere displays a dipole structure, and points westward within the heating region. Despite these similarities, the stream function displays a sensitivity to α^2. As this parameter increases, the stream function decreases more rapidly along the zonal direction, but decreases more slowly in the meridional direction. It also decreases in amplitude, which suggests a weakening of horizontal velocity as radiation increases relative to momentum damping.

In figures 11 and 12, we plot the zonal and meridional velocities at the bottom of the troposphere for increasing values of α^2. As was the case for zero radiation, at the bottom of the troposphere, the velocity flows into the heating region. Since the horizontal velocity is anti-symmetric about the mid-troposphere, the circulation is directed out of the heating region at the top of the troposphere. As α^2 increases, the zonal velocity becomes more eccentric along the

meridional direction while becoming weaker. Note, also, that the meridional velocity responds to increasing α^2 in the same way as the stream function does in the mid-troposphere. This is to be expected, however, because from equation (3), the meridional velocity is proportional to Φ_y, and as was shown in (Marsico *et al.* 2023), the stream function is related to the velocity potential by equation (23).

4. Diffusive Momentum Damping and Newtonian Cooling

In this section, we look at the case when $d_1 = -\mu\nabla^2$. As was shown in (Marsico *et al.* 2023), the vertical potential and vertical velocity satisfy the equations

$$\nabla^2\nabla_h^2\Phi - \frac{\mu d_2}{N^2}\nabla^6\Phi - \frac{4\Omega^2}{N^2}\frac{d_2}{\mu}\left(\cos(\theta)\frac{\partial}{\partial y} + \sin(\theta)\frac{\partial}{\partial z}\right)^2\Phi = \frac{1}{N^2}\nabla^2 S_z \tag{58}$$

and $w_z = \nabla_h^2\Phi$. At the equator, a straightforward non-dimensionalization shows that the sixth order derivative on the left hand side of equation (58) is small relative to the second and fourth order terms, and when neglected, equation (58) becomes

$$\nabla^2\nabla_h^2\Phi - \frac{4\Omega^2}{N^2}\frac{d_2}{\mu}\Phi_{yy} = \frac{1}{N^2}\nabla^2 S_z. \tag{59}$$

We do not attempt to find exact analytic solutions for Φ or w, but rather we compute solutions numerically. As in the analytic example above, we again assume that S is of the form $S = S_0\,\Theta(x,y)\sin(\pi z/H)$, The velocity potential is of the form

$$\Phi = \frac{\pi S_0}{HN^2}B(x,y)\cos(\pi z/H), \tag{60}$$

where $B(x,y)$ satisfies

$$\nabla_h^4 B - \left(\frac{\pi^2}{H^2}\right)\nabla_h^2 B - \frac{4\Omega^2}{N^2}\frac{d_2}{\mu}B_{yy} = \nabla_h^2\Theta - \left(\frac{\pi^2}{H^2}\right)\Theta, \tag{61}$$

which we solve by numerical inversion of the elliptic operator on the left hand side. In figure 13, the velocity potential is plotted as a function of the non-dimensional parameter λ^2, where

$$\lambda^2 = \frac{4\Omega^2}{N^2}\frac{d_2}{\mu}H^2. \tag{62}$$

In figure 13, we plot the velocity potential as a function of λ^2. Observe that as λ^2 increases, that is, as the effects of radiation become stronger, the velocity potential becomes highly anisotropic. Similar behavior occurs in the case of linear momentum damping.

In figure 14, we plot the vertical velocity as a function of λ^2. For small values of λ^2, the vertical velocity is localized to the heating region. As λ^2 increases, the velocity becomes negative along the equator, and positive poleward. This is again similar to what occurs in the case of linear momentum damping. Hence, the linear approximation to momentum damping yields a similar response to increased radiation relative to momentum damping as the diffusive approximation to momentum damping.

It is also important to recognize the role of radiation. As was the case for linear momentum and radiative damping, in the case of diffusive momentum damping the vertical velocity satisfies the WTG approximation in the absence of radiation. Thus it is radiative cooling that allows the non-traditional Coriolis force to have an impact on the convective circulation, (w, Φ), causing the convection to respond to the heating in areas where there is no heating (i.e. non-locally).

5. Synthesis

In this section, we contrast the velocity potential given by equations (5), (19), and (58). In the absence of radiation, the velocity potential is independent of the Coriolis force. Rotation is present only in the equation for the stream function, and therefore its effect is seen only in the horizontal velocities; the response of the vertical velocity to localized heating remains local, that is to say, vertical velocity is non-zero only where heating is non-zero. However, in the presence of radiation, rotation is folded back into the equation for velocity potential, and the response of the vertical velocity to localized heating becomes non-local. In particular, there exist regions away from the heating region where the flow ascends and descends. This is a potential explanation for the horizontal growth of precipitating systems in previous three dimensional modeling studies which included the NCT (and radiation) (Igel and Biello 2020, Liang and Chan 2005)

In the two cases where radiation is present, the parameters α^2 (equation (25)) and λ^2 (equation (62)) are the important parameters for determining the structure of the atmospheric response to localized heating. These terms are composed of a pair of ratios: the square of the ratio of the buoyancy forcing timescale to that of the Coriolis parameter, and the ratio of the radiative damping to the momentum damping. The response of the atmosphere to a localized source of heating is most pronounced for large α^2 and λ^2, as can be seen in the asymmetry of the meridional and zonal structure of the flow in figures 5 and 13. We expect such flows to occur occur for weak stratification, weak momentum damping, or high radiative damping, each of which would correspond to a high value of α^2 or λ^2.

Overall, the results presented above imply that rising air inside a region of thermal forcing and the environmental air in which it is embedded interact in a number of important ways in the presence of the NCT and radiation that are not considered in traditional treatments (e.g. Arakawa and Schubert (1974)). The upward and downward flows are connected meaningfully and feedback on one another. Broadly speaking, such feedbacks between cloudy and environmental air are crucial to developing complex flow morphologies characteristic of real-world clouds (Houze Jr. 2004). We can see clearly from Figures 6 and 14 that the shape of convection can change from round, reminiscent of an isolated convective tower, to linear, reminiscent of a squall line, with increasing α^2 or λ^2. Changes to morphology of convection result in consequential changes to impacts like convective momentum transport which has previously been observed to depend on the NCT (Lemone 1983). In what we have developed here, the effect of the NCT on convective momentum transport can be seen by examining the vertical transport of zonal momentum, uw, in the absence of radiation. Considering a heating of the form used in section 2 (constant on the interior of a disk and zero outside), the vertical transport of zonal momentum is

$$uw = \begin{cases} -\dfrac{x}{2N^4} f'(z) f(z) - \dfrac{\Omega}{d_1 N^4} f^2(z) & \text{if } r^2 < L^2 \\ 0 & \text{else,} \end{cases} \tag{63}$$

where we have used equation (10), and the fact that in the absence of radiation, $w = f(z)/N^2$. Now we are ultimately interested in the horizontal average, $\overline{uw}$, as this term contributes to the feed back of convective circulations onto larger scales. Integrating equation (63) about a disk of radius L shows that in the absence of rotation (equivalent to taking $\Omega = 0$), $\overline{uw} = 0$. In the presence of rotation, however, $\overline{uw}$ is equal to a non-zero constant. Thus, the NCT provides a mechanism for sub-grid convective flows to force mean or grid-scale flows. The implications of this, as well as a detailed discussion of momentum transport induced by the steady state circulations studied here, is the subject of future work.

6. Conclusion

We have solved the systems of equations derived in Part I (Marsico *et al.* 2023) which describe the linear atmospheric response to heating, damping, radiation and Coriolis force. Our solutions show the response of a tropical atmosphere to an imposed horizontally localized, positive signed heating. These solutions are relevant across a wide range of length scales and timescales long enough that the steady state assumption is reasonable (Marsico *et al.* 2023).

For solutions in the absence of radiation, the non-traditional Coriolis Force begets a secondary horizontal circulation whose intensity is inversely proportional to the strength of the momentum damping. In the presence of radiative damping, regardless of the form of the momentum damping, strong zonal-meridional asymmetries develop as the intensity of the radiative damping increases. The radiation causes the Coriolis force to modify the convective circulation (w, Φ), and results in a non-local response of the vertical velocity to a localized heating.

Our conclusion that the non-traditional Coriolis terms should not be ignored in cases of weak stratification has been obtained by several previous authors (Liang and Chan 2005, Hayashi and Itoh 2012, Ong and Roundy 2019, 2020, Igel and Biello 2020, Ong and Yang 2022). However, the interaction of the NCT with radiation is a unique result of our analysis. The actual tropical atmosphere is certainly more complicated than equations (2a)-(2e) and therefore more complicated than our solutions suggest. But together, our conclusions suggest that the NCT should be most important in moist convecting systems with weak stratification and potentially strong radiative effects.

References

Arakawa, A. and Schubert, W., Interactions of a Cumulus Cloud Ensemble with the Large-scale Environment, Part I. *Journal of the Atmospheric Sciences*, 1974, **31**, 674–701.

Hayashi, M. and Itoh, H., The Importance of the Nontraditional Coriolis Terms in Large-Scale Motions in the Tropics Forced by Prescribed Cumulus Heating. *Journal of the Atmospheric Sciences*, 2012, **69**, 2699–2716.

Helmholtz, H., On Integrals of the hydrodynamical equations, which express vortex-motion. *The London, Edinburgh, and Dublin Philosophical Magazine and Journal of Science*, 1867, **33**, 485–512.

Hittmeir, S. and Klein, R., Asymptotics for moist deep convection I: Refined scalings and self-sustaining updrafts. *Theor. & Comput. Fluid Dyn.*, 2018, **32**, 137–164.

Houze Jr., R.A., Mesoscale Convective Systems. *Reviews of Geophysics*, 2004, **42**, RG4003.

Igel, M.R. and Biello, J.A., The Nontraditional Coriolis Terms and Tropical Convective Clouds. *Journal of the Atmospheric Sciences*, 2020, **77**, 3985–3998.

Jeevanjee, N. and Romps, D.M., Effective buoyancy at the surface and aloft. *Quarterly Journal of the Royal Meteorological Society*, 2016, **142**, 811–820.

Lebovitz, N.R., The stability equations for rotating, inviscid fluids: Galerkin methods and orthogonal bases. *Geophysical & Astrophysical Fluid Dynamics*, 1989, **46**, 221–243.

Lemone, M.A., Momentum transport by a line of cumulonimbus. *Journal of the Atmospheric Sciences*, 1983, **40**, 1815–1834.

Liang, X. and Chan, J.C.L., The Effects of the Full Coriolis Force on the Structure and Motion of a Tropical Cyclone. Part I: Effects due to Vertical Motion. *Journal of the Atmospheric Sciences*, 2005, **62**, 3825–3830.

Marsico, D.H., Biello, J.A. and Igel, M.R., The Weak Temperature Gradient on Convective Scales. Part I: A Framework for Assessing Radiation the Coriolis Force and Drag. *Journal of the Atmospheric Sciences*, 2023.

Ong, H. and Roundy, P.A., Linear effects of nontraditional Coriolis terms on intertropical convergence zone forced large-scale flow. *Quarterly Journal of the Royal Meteorological Society*, 2019, **145**, 2445–2453.

Ong, H. and Roundy, P.E., Nontraditional hypsometric equation. *Quarterly Journal of the Royal Meteorological Society*, 2020, **146**, 700–706.

Ong, H. and Yang, D., The compressional beta effect and convective system propagation. *Journal of the Atmospheric Sciences*, 2022, **79**, 2031 – 2040.

Romps, D.M. and Charn, A.B., Sticky Thermals: Evidence for a Dominant Balance between Buoyancy and Drag in Cloud Updrafts. *Journal of the Atmospheric Sciences*, 2015, **72**, 2890 – 2901.

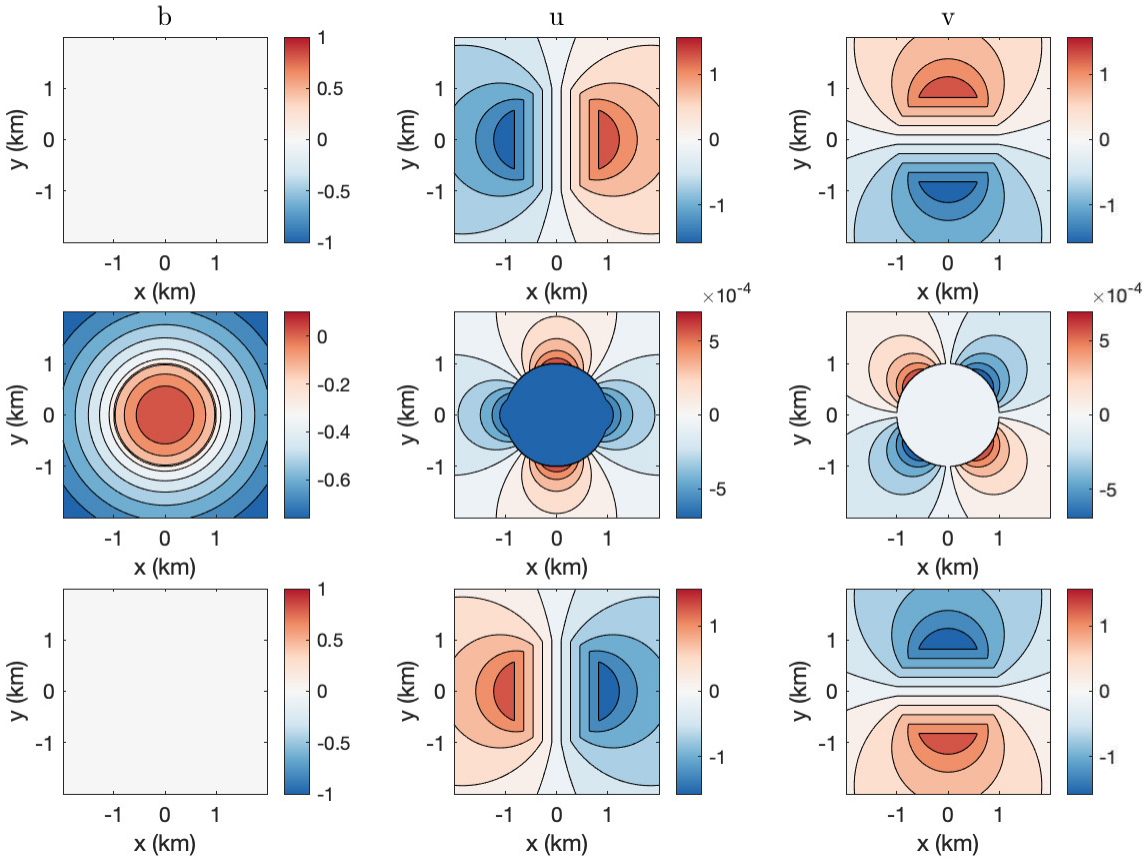

Figure 1. Horizontal cross sections of the buoyancy, zonal, and meridional velocities at three different heights, for $d_1 = 0.1\,s^{-1}$, and no radiation. The bottom row is for $z = 0$, the middle row is for $z = H/2$, and the top row is $Z = H$. The spatial domain has been scaled to the height of the troposphere $H = 15$ km. Note that the buoyancy is identically zero at the bottom and top of the troposphere (colour online).

Appendix A: Appendix

In this section, we write down an explicit expression for the horizontal dependence of the vertical velocity that results from the localized heating that appears in equation (57). The solution in the interior of the circle of radius L is denoted by w_{interior} and the solution in the exterior is denoted by w_{exterior}. To determine w_{exterior}, we differentiate equation (51) with respect to Y:

$$F_Y = \frac{L^2}{2(2+\alpha^2)}\left[\frac{2+\alpha^2}{\sqrt{1+\alpha^2}} - \frac{\alpha^2}{\sqrt{1+\alpha^2}}\cosh(2\mu_0)e^{-2\mu}\cos(2\nu)\right]\mu_Y - \frac{L^2\alpha^2}{2(2+\alpha^2)\sqrt{1+\alpha^2}}\cosh(2\mu_0)e^{-2\mu}\sin(2\nu)\nu_Y \tag{A.1}$$

$$\begin{aligned} F_{YY} = {} & \frac{\alpha^2 L^2}{(2+\alpha^2)\sqrt{1+\alpha^2}}\cosh(2\mu_0)e^{-2\mu}\left[\cos(2\nu)\mu_Y + \sin(2\nu)\nu_Y\right]\mu_Y \\ & + \frac{L^2}{2(2+\alpha^2)\sqrt{1+\alpha^2}}\left[2+\alpha^2-\alpha^2\cosh(2\mu_0)e^{-2\mu}\cos(2\nu)\right]\mu_{YY} \\ & - \frac{L^2\alpha^2}{(2+\alpha^2)\sqrt{1+\alpha^2}}\cosh(2\mu_0)e^{-2\mu}\left[-\sin(2\nu)\mu_Y\nu_Y + \cos(2\nu)\nu_Y^2 + \frac{1}{2}\sin(2\nu)\nu_{YY}\right] \end{aligned} \tag{A.2}$$

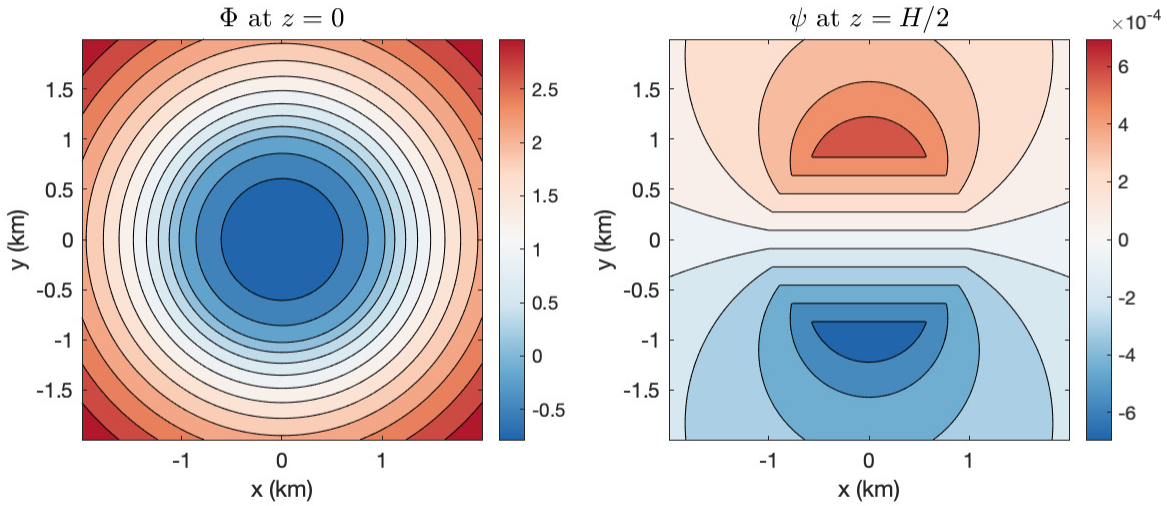

Figure 2. The velocity potential, Φ, at a height of $z = 0$, and stream function, ψ, at height of $z = H/2$. Both functions are for the case of $d_1 = 0.1s^{-1}$, and no radiation. The velocity and stream function have been normalized to the height of the troposphere, and both are plotted on a spatial domain that has been scaled to the height of the troposphere H as well (colour online).

Equation (A.2) is complete once we determine ν_Y, μ_Y, ν_{YY}, and μ_{YY}. To determine ν_Y, we differentiate the equation

$$\left(\frac{x}{\gamma\cos(\nu)}\right)^2 - \left(\frac{Y}{\gamma\sin(\nu)}\right)^2 = 1 \tag{A.3}$$

with respect to Y, where

$$\gamma = \frac{\alpha L}{\sqrt{1+\alpha^2}}. \tag{A.4}$$

This results in the equation

$$\frac{2x^2\sin(\nu)\nu_Y}{\gamma^2\cos^3(\nu)} - \frac{2\gamma^2 Y\sin^2(\nu) - 2\gamma^2 Y^2\cos(\nu)\sin(\nu)\nu_Y}{\gamma^4\sin^4(\nu)} = 0. \tag{A.5}$$

After simplifying, we obtain the following expression for ν_Y:

$$\nu_Y = \frac{Y\cos^3(\nu)\sin(\nu)}{x^2\sin^4(\nu) + Y^2\cos^4(\nu)} \tag{A.6}$$

To determine μ_Y, we differentiate the equation

$$\left(\frac{x}{\gamma\cosh(\nu)}\right)^2 + \left(\frac{Y}{\gamma\sinh(\nu)}\right)^2 = 1 \tag{A.7}$$

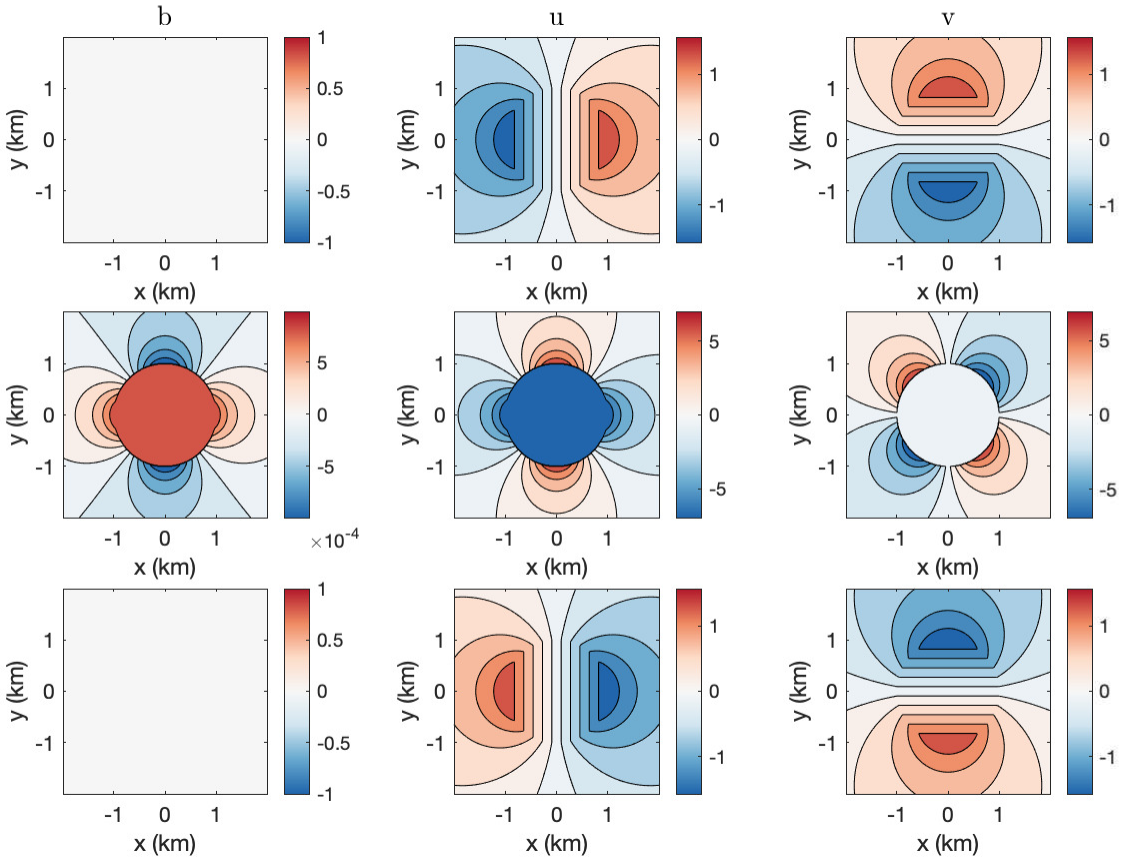

Figure 3. Horizontal cross sections of the buoyancy, zonal, and meridional velocities at three different heights, for $d_1 = 10^{-5}\, s^{-1}$, and no radiation. The bottom row is for $z = 0$, the middle row is for $z = H/2$, and the top row is $Z = H$. The spatial domain has been scaled to the height of the troposphere $H = 15$ km. Note that the buoyancy is identically zero at the bottom and top of the troposphere (colour online).

with respect to Y. This results in

$$\frac{-2x^2 \sinh(\mu)\mu_Y}{\gamma^2 \cosh^3(\mu)} + \frac{2Y\gamma^2 \sinh^2(\mu) - 2\gamma^2 Y^2 \sinh(\mu)\cosh(\mu)\mu_Y}{\gamma^4 \sinh^4(\mu)} = 0, \tag{A.8}$$

which, after simplifying, becomes

$$\mu_Y = \frac{Y \cosh^3(\mu)\sinh(\mu)}{x^2 \sinh^4(\mu) + Y^2 \cosh^4(\mu)}. \tag{A.9}$$

The derivatives ν_{YY} and μ_{YY} are then obtained by differentiating equations (A.6) and (A.9). The vertical velocity in the exterior is then given by the equation

$$w_{\text{exterior}} = S_0 - \frac{S_0\alpha^2}{1+\alpha^2} F_{YY} \tag{A.10}$$

where S_0 is a constant, and F_{YY} is given by equation (A.2). The expression the w_{interior} is simpler. It is obtained by differentiating equation (53), and is given by the equation

$$w_{\text{interior}} = S_0 - \frac{S_0\alpha^2}{(1+\alpha^2)(2+\alpha^2)}(1+\alpha^2-\sqrt{1+\alpha^2}) \tag{A.11}$$

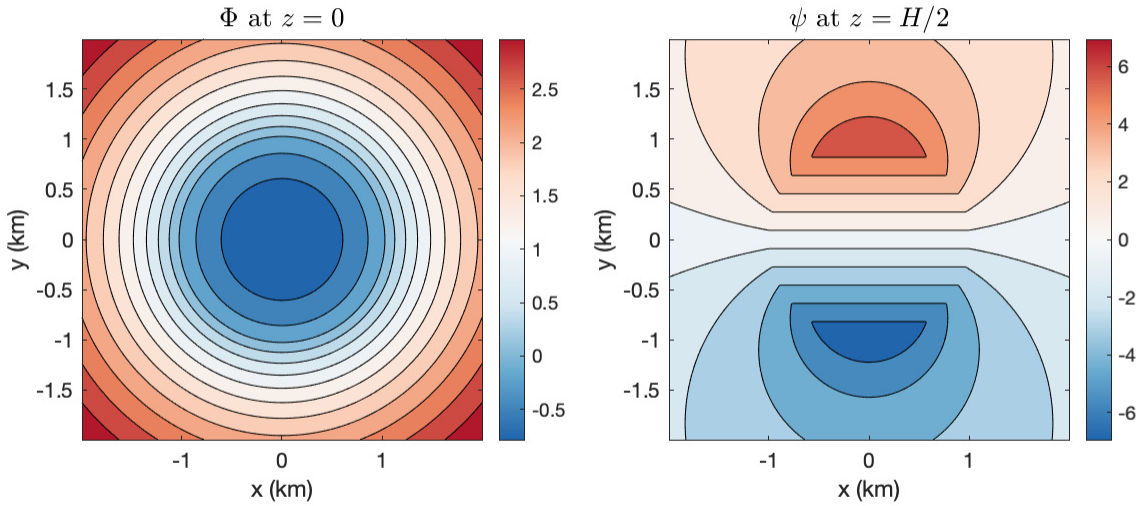

Figure 4. The velocity potential, Φ, is shown at a height of $z = 0$. The stream function, ψ, is shown at height of $z = H/2$. Both functions are for the case of $d_1 = 10^{-5}s^{-1}$. The velocity and stream function have been normalized to the height of the troposphere, and both are plotted on a spatial domain that has been scaled to the height of the troposphere H as well (colour online).

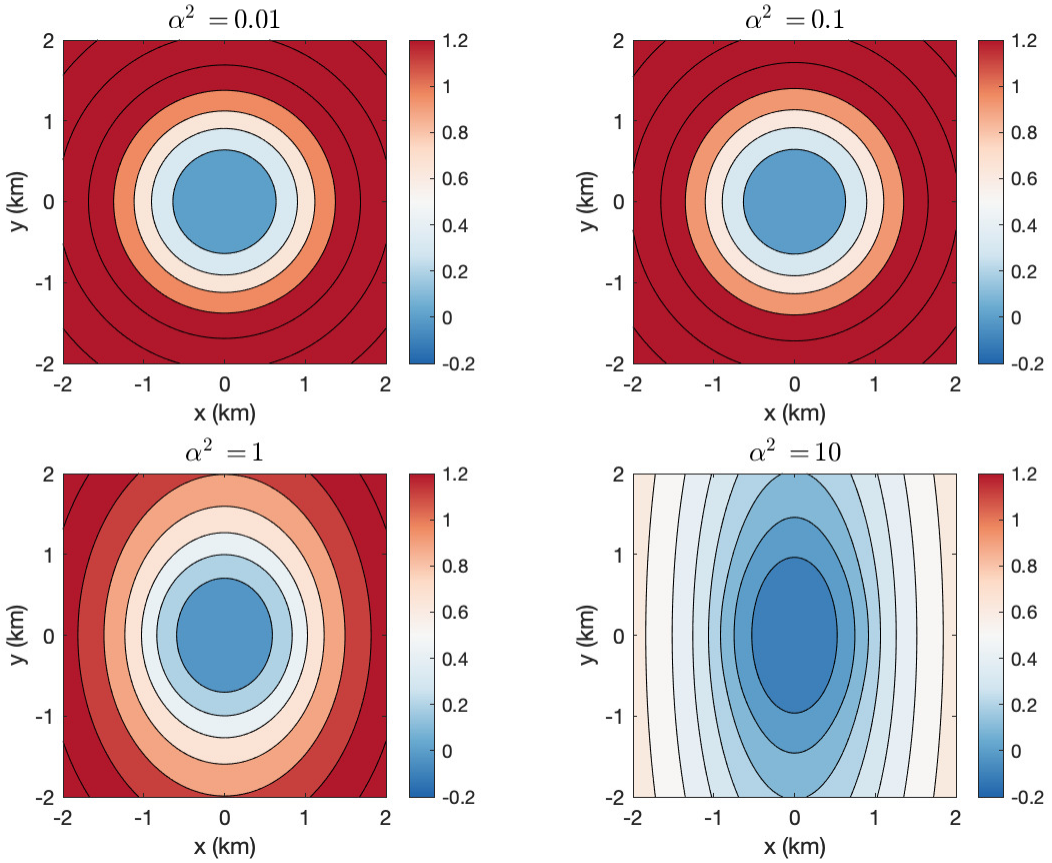

Figure 5. The velocity potential at the bottom of the troposphere, $z = 0$, for increasing values of α^2, in the case of linear momentum drag and radiation (colour online).

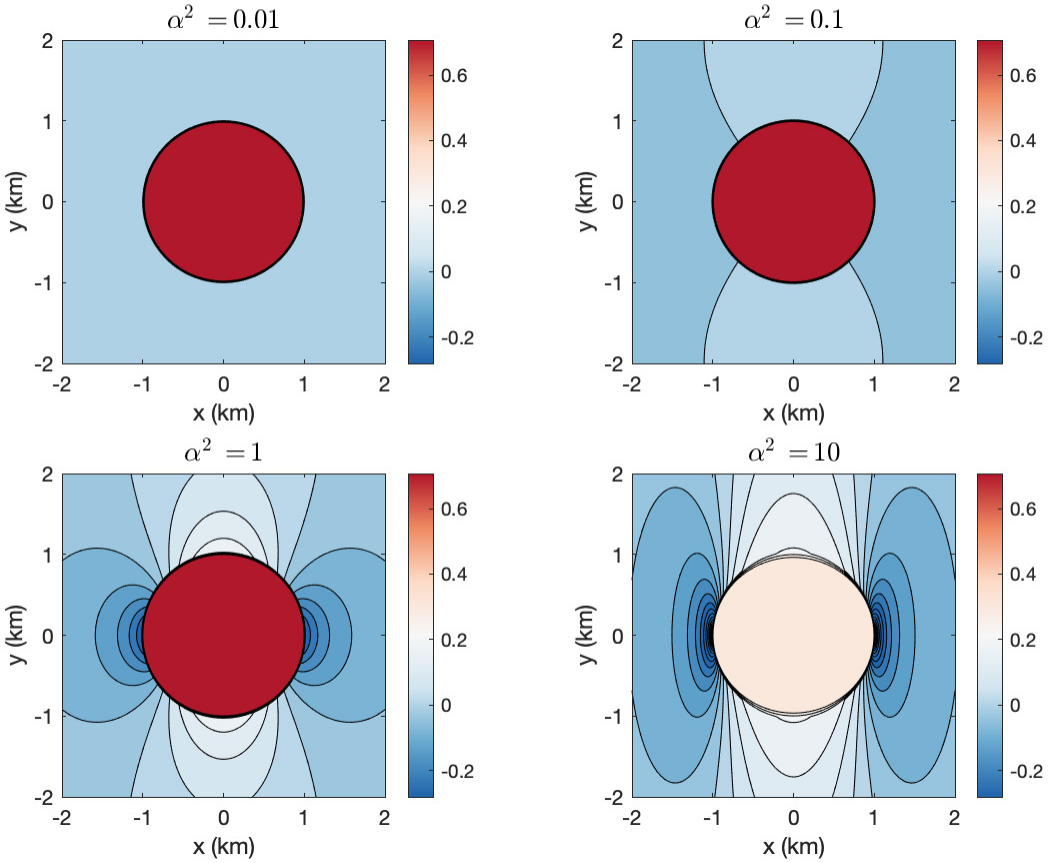

Figure 6. The vertical velocity in the mid-troposphere, $z = H/2$, for increasing values of α^2, in the case of linear momentum drag and radiation (colour online).

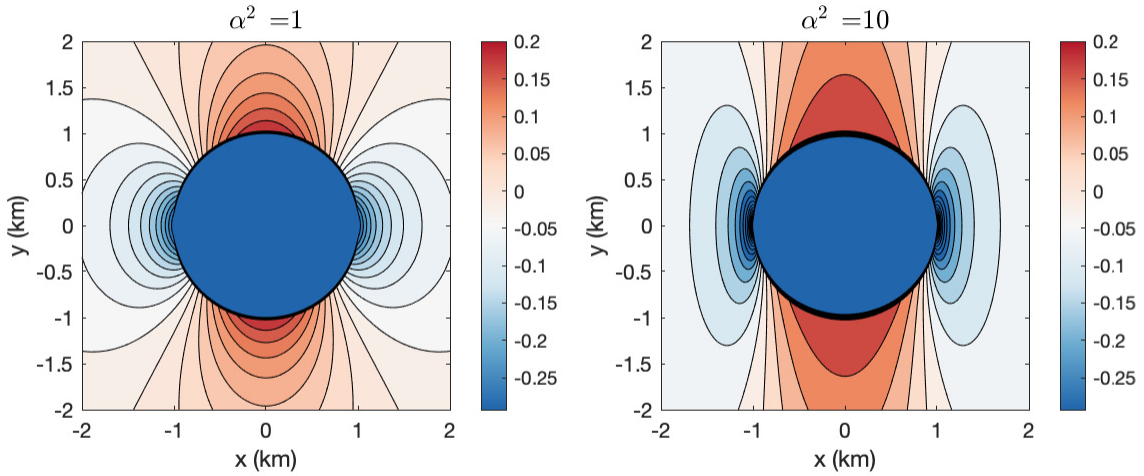

Figure 7. The vertical velocity in the mid-troposphere, $z = H/2$, shown as the deviation from the WTG solution (constant in the interior, and zero in the exterior). The deviation from the WTG solution for $\alpha^2 = 0.01$ and $\alpha^2 = 0.1$ is effectively zero, and so we only show the plots for $\alpha^2 = 1$ and $\alpha^2 = 10$ (colour online).

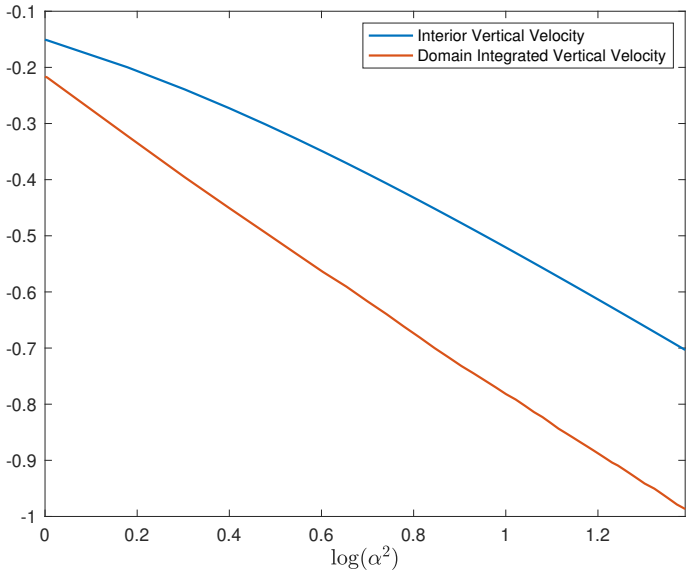

Figure 8. The domain integrated vertical velocity and interior vertical velocity are plotted as a functions of α^2, on a log-log scale, in the case of linear momentum drag and radiation. The domain integrated vertical velocity is normalized by the area of the heating region so that it is equal to the interior vertical velocity for $\alpha^2 = 0$ (colour online).

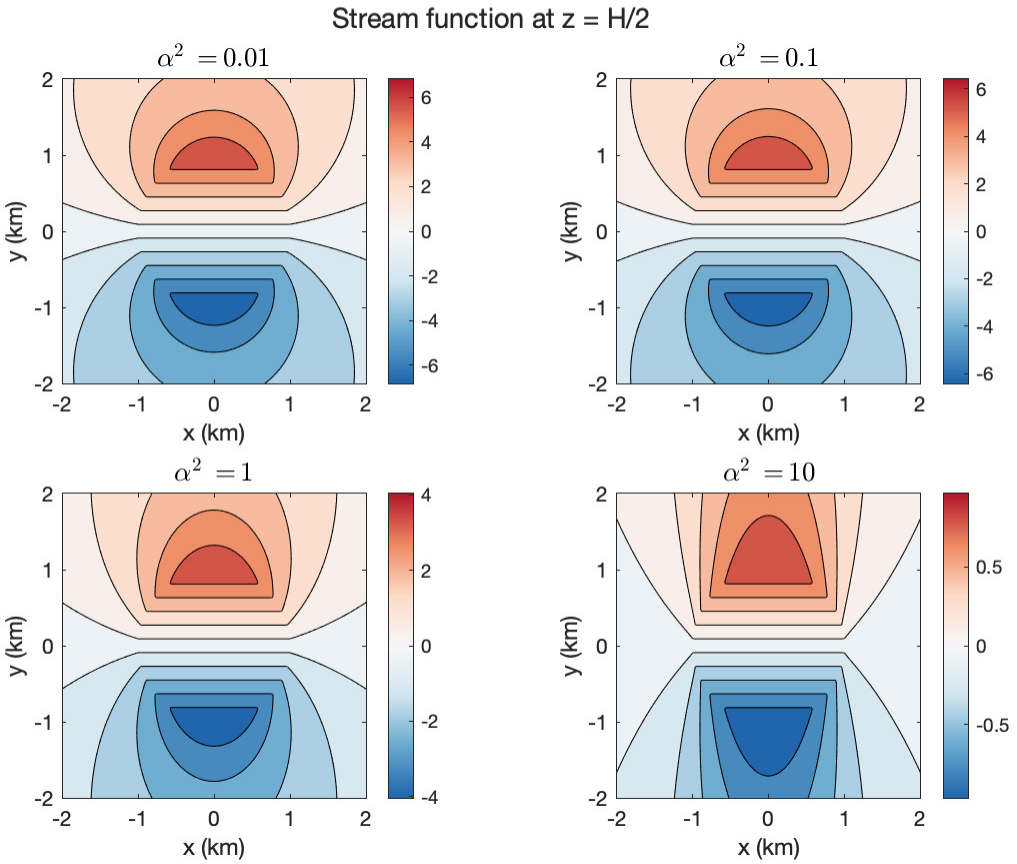

Figure 9. The stream function, ψ, in the mid-troposphere ($z = H/2$) in the case of linear momentum and radiative damping for $d_1 = 10^{-5}\, s^{-1}$, shown for increasing values of α^2 (colour online).

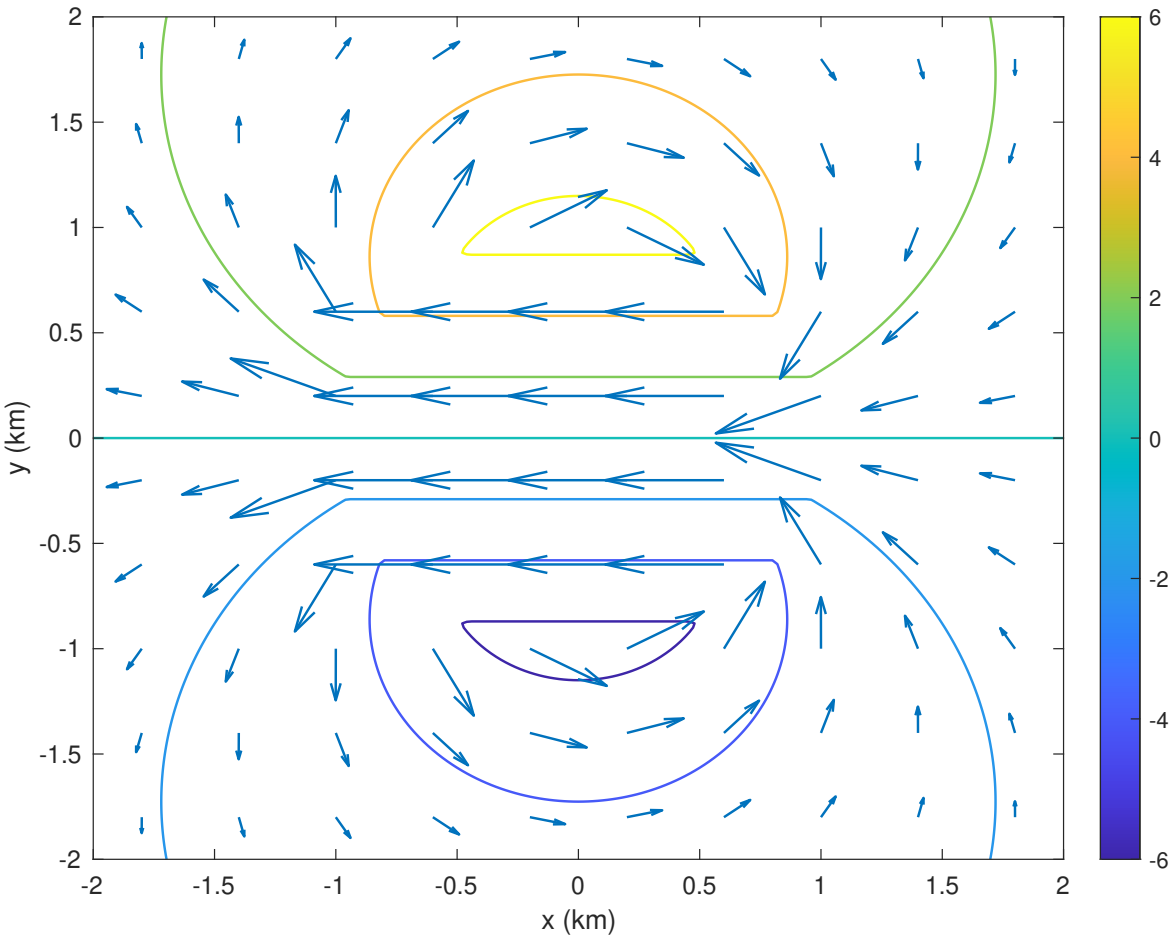

Figure 10. The solid contours show the stream function, ψ, and the horizontal velocity vector field in the mid-troposphere ($z = H/2$) in the case of linear momentum and radiative damping for $d_1 = 10^{-5}\ s^{-1}$ (colour online).

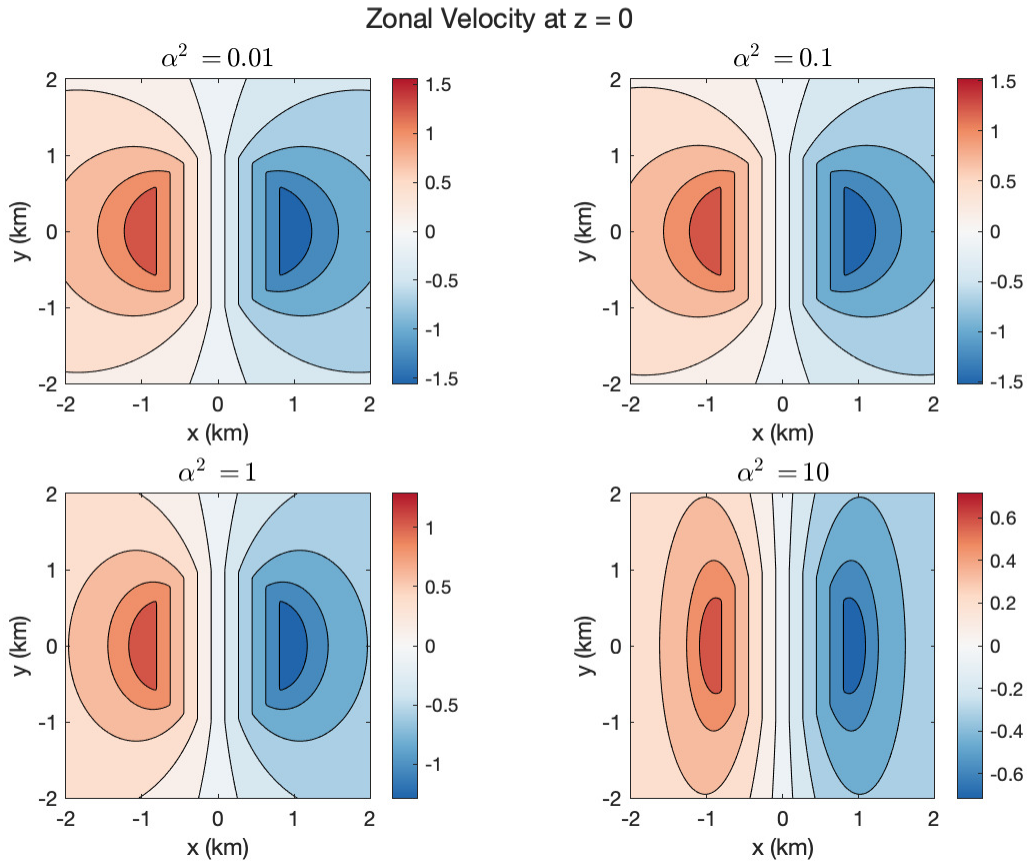

Figure 11. The zonal velocity, u, at the bottom of the troposphere ($z = 0$), for $d_1 = 10^{-5}\, s^{-1}$, shown for increasing values of α^2 (colour online).

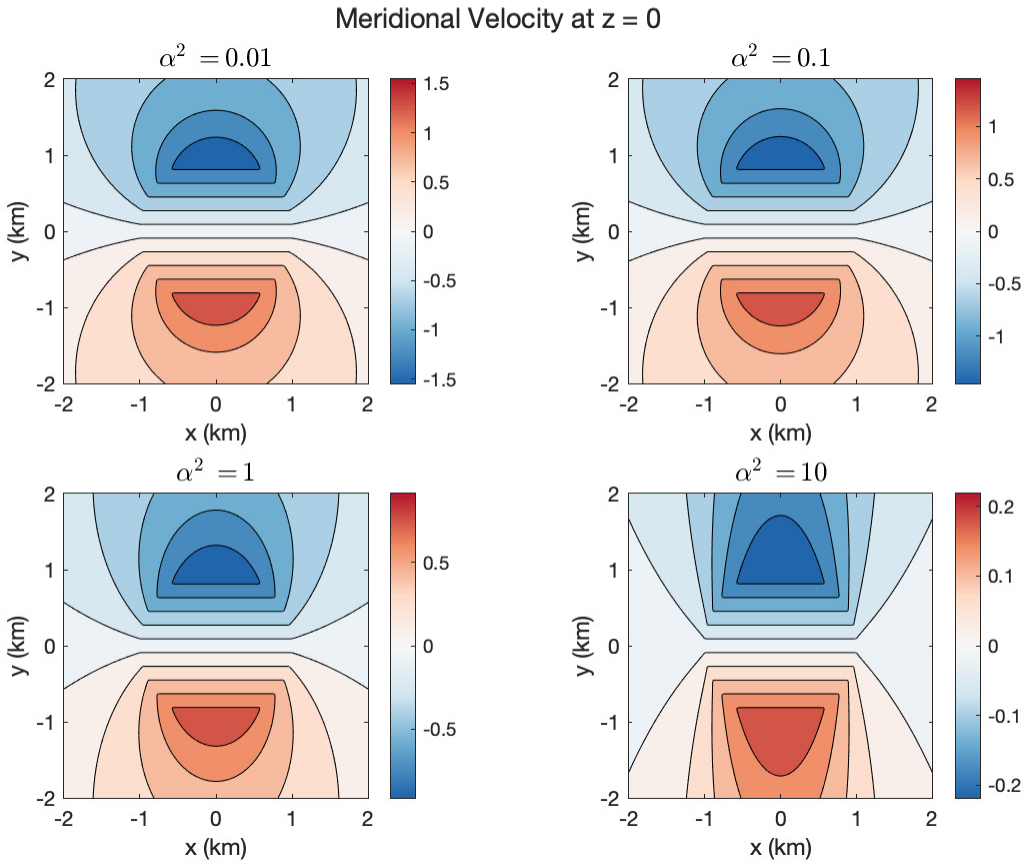

Figure 12. The meridional velocity, u, at the bottom of the troposphere ($z = 0$), for $d_1 = 10^{-5}\, s^{-1}$, shown for increasing values of α^2 (colour online).

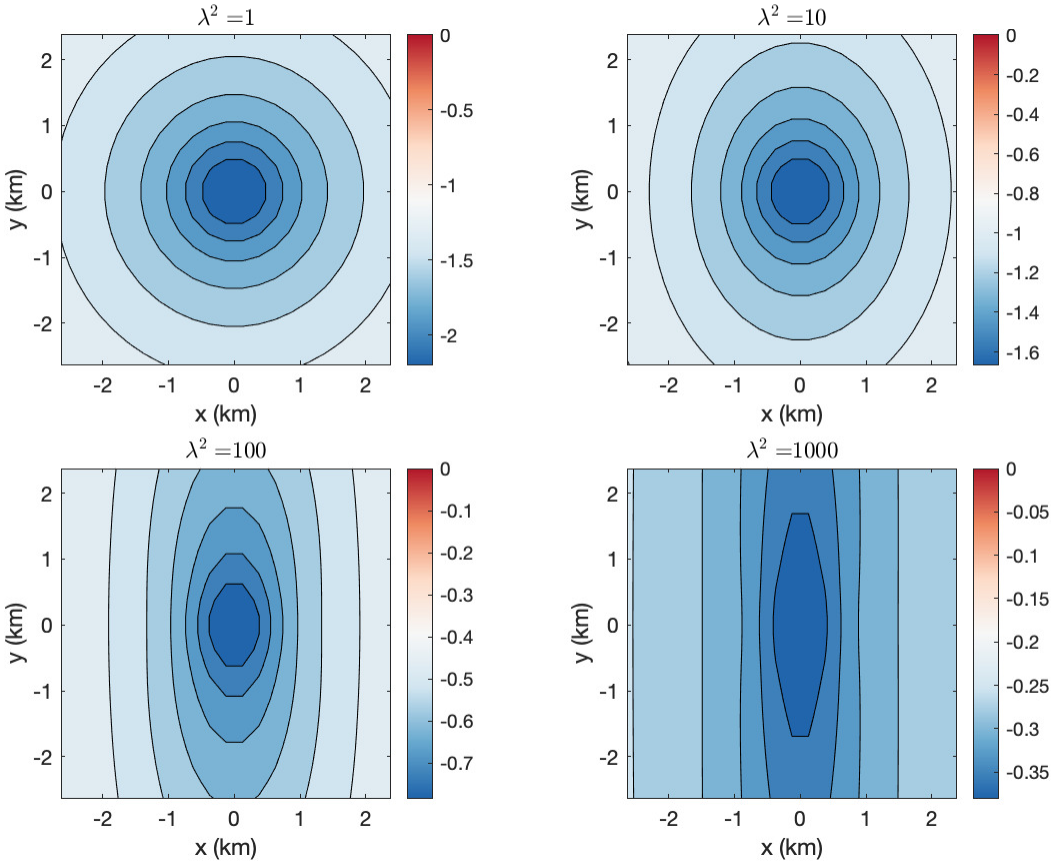

Figure 13. The velocity potential at the bottom of the troposphere ($z = 0$), for linear radiation and diffusive damping for increasing values of λ^2 (colour online).

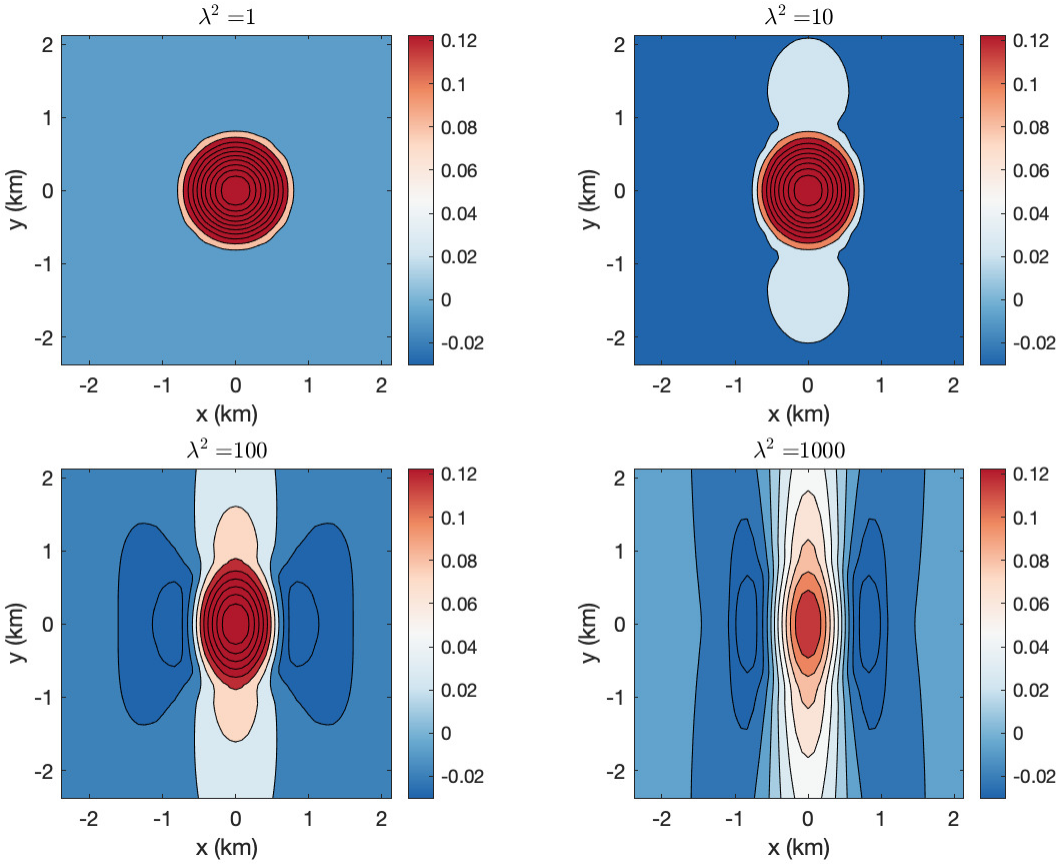

Figure 14. The vertical velocity in the mid-troposphere ($z = H/2$), for linear radiation and diffusive damping for increasing values of λ^2 (colour online).